A spatial Monte Carlo model of IP_3-dependent calcium oscillations

Evan Molinelli

Advisor: Gregry D. Smith

Department of Applied Science

The College of William and Mary

Williamsburg, VA 23187

4/14/06

1 Introduction

As a newcomer to computational cell biology, I spent the entirety of the first semester and much of second semester learning about modeling techniques using Matlab, the physiology of intracellular calcium dynamics, and the various types of models already in use. To begin with I learned about Euler's explicit method and the Crank-Nicholson implicit method for numerically solving diffusion equations and implemented these methods in a Matlab code to model the one dimensional spatio-temporal "cable equation". By the end of first semester, I had a spatially extended (in one dimension) model of intracellular Ca^{2+} concentration ($[Ca^{2+}]$) that included stochastic independently gating two-state channels. While the formulation of this model was crucial to the development of my understanding of models of intracellular Ca^{2+} handling, it was preliminary work. The main goal of my research was to conduct a parameter study to compare two different modeling approaches used in the study of intracellular $[Ca^{2+}]$ oscillations.

Dr. Smith was interested in testing a specific model that he and a graduate student, Blair Williams, had recently developed. This model utilized a so-called "probability density approach" (PDA) to track the probability of channel opening. [5] However, the method does not explicitly account for the spatial dependence of $[Ca^{2+}]$ in cells. To determine the validity of neglecting spatial aspects in the PDA model, I created a corresponding model that explicitly included one spatial dimension to serve as the standard by which the Monte Carlo version of Blair's probability density model could can be compared.

I shall organize the rest of the paper in the following way. First, I will introduce some background information about Ca^{2+} dynamics and intracellular Ca^{2+} channel modeling. I will then briefly introduce the complete spatio-temporal model developed in Fall 2005 -

Spring 2006. Next, I will discuss the comparison of my full spatial model to Blair's non-spatial reduced model. Finally, I will present results and conclusions concerning the agreement and disagreement between the two approaches.

2 Background: Calcium Dynamics

There are various kinds of intracellular calcium behaviors such as spiking, regular oscillations, waves, puffs, and sparks. The type of behavior observed in living cells is dependent on the type(s) of plasma membrane and intracellular Ca^{2+} channels involved, the distribution of channels along the endoplasmic reticulum (ER) membrane, and the kinetics of channel gating. Here we are focused on oscillations of cytosolic calcium concentration ($[Ca^{2+}]_{cyt}$) as a function of time due to release from ER stores through intracellular calcium channels. These oscillations are crucial to cell signaling and are therefore important to model accurately and understand.

The two physiological compartments in the models presented below are the cytosol and the ER. The Ca^{2+} concentration in the ER is much higher than that of the cytosol, but the volume of the cytosol is much larger than that of the ER. Since we will be dealing with a closed cell model in which Ca^{2+} ions can neither enter nor leave the cell by traversing the plasma membrane, $[Ca^{2+}]_{cyt}$ can only change when Ca^{2+} ions flow between the cytosol and ER. These two compartments are separated by the ER membrane that contains Ca^{2+} channels, through which Ca^{2+} ions diffuse from the ER into the cytosol. The two main Ca^{2+} channels are the ryanodine receptor Ca^{2+} channels (RyR) and the inositol 1,4,5-trisphosphate receptor (IP_3R), each with their own unique gating properties. [1] Both the PDA model and the spatio-temporal model will be using the gating properties of IP_3R channels. Gating is

the process by which channels change state according to their specific transition properties. Gating properties of Ca^{2+} channels include the transition rates into and out of the allowed channel states as well as any Ca^{2+} dependencies of these transition rates. The gating properties of the IP_3R channels will be discussed and detailed later in section 2.3.

In the closed cell model, there are only three fluxes that contribute to changes in $[Ca^{2+}]_{cyt}$. The first flux term, J_{pump}, flows against the resting Ca^{2+} concentration gradient and pumps Ca^{2+} ions from the cytosol into the ER. The transporters responsible for this pumping of Ca^{2+} ions against the concentration gradient to replenish $[Ca^{2+}]_{ER}$ are called the sacroplasmic/endoplsamic reticulum Ca^{2+} ATPases (SERCA pumps). The second flux term, J_{leak}, is a leakage flux directly proportional to the difference in concentration between the ER and cytosol. The third and final flux term, J_{rel}, is also proportional to the Ca^{2+} concentration difference between the ER and cytosol. Unlike the other two fluxes, J_{rel} is dependent on the presence and specific location of Ca^{2+} channels along the length of the ER membrane. That is, the Ca^{2+} ions carried by J_{rel} can only flow when IP_3Rs are located at that spatial position and only when these channels are in the permissive or open state.

2.1 The four compartment model

So far, we have been considering a two compartment model of intracellular Ca^{2+} handling. While we are only considering $[Ca^{2+}]$ in two membrane-deliniated compartments (the ER and cytosol), to accurately represent certain aspects of the dynamics of local Ca^{2+} signaling near clusters of IP_3Rs the Smith lab often introduces two additional compartments in order to distinguish between the Ca^{2+} concentration in areas far away from intracellular Ca^{2+} and the Ca^{2+} concentration in areas nearer the channels. Immediately following

channel opening, Ca^{2+} ions from the ER flow into the cytosol, therefore it is reasonable to assume that the concentration just outside this open channel is effectively higher than the concentration in the rest of the cytosol or ER. We call the areas far away from the channels the "bulk", and the areas near the channels the "domains". Hence, the compartmental modeling that follows includes a bulk cytosol concentration ($[Ca^{2+}]_{cyt}$), a bulk ER concentration ($[Ca^{2+}]_{ER}$), a domain cytosolic concentration ($[Ca^{2+}]^d_{cyt}$) and a domain ER concentration ($[Ca^{2+}]^d_{ER}$).

When we are only dealing with two compartments, there was only one flux (J_{rel}) that was dependent on the location and state of channels along the ER membrane. In this four-compartment model, we must divide that original flux into three separate but related and interdependent fluxes. The first new flux (J_{er}) flows between the bulk ER and the domain ER. When the channel is open, Ca^{2+} ions flow between the two domain compartments via (J_{rel}) at a rate proportional to the concentration gradient between the two domains. Finally, there is a flux between the domain cytosol and the bulk cytosol (J_{cyt}). The bulk concentration is only increased by J_{cyt}, while the values of J_{cyt} will depend on the cascading effects of J_{er} and J_{rel}. Note that each of these four compartments are spatially extended along the length of the membrane. See Figure 1 for a visual representation of the four -compartment model.

Figure 1: Visual representation of the four-compartment model. The black horizontal line represents the ER membrane.

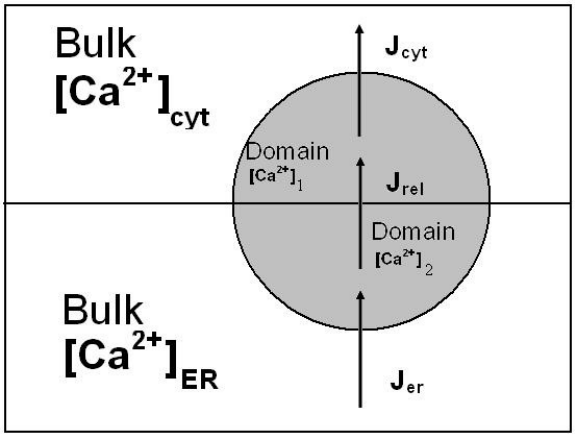

2.2 Stochastic and Deterministic Modeling Approaches

Models of intracellular Ca^{2+} signaling can be either deterministic or stochastic. Deterministic models are often governed by a system of coupled differential equations and each simulation with identical parameters ought to yield exactly the same results. To simulate deterministic systems, one need only to insert the differential equations and parameters into an ODE solving program (e.g. XPP or Matlab) and plot the results. These packages provide various options allowing the user to select a numerical method (e.g. forward Euler) appropriate for the ODE system of interest. Conversely, stochastic models always involve at least one random variable.

The spatial model of intracellular Ca^{2+} handling that I developed this year is a stochastic model, but the stochastic aspect is restricted to one compartment: the gating of the intracellular Ca^{2+} channels. It is conventional and experimentally supported to model the gating of intracellular Ca^{2+} channels in a stochastic fashion. In fact, it is important to do so when the number of intracellular Ca^{2+} is small. In other respects the model is deterministic, for

example, the diffusion of Ca^{2+} along the length of the cell in the cytosolic and ER compartments is simulated using a system of deterministic nonlinear ODEs. The following section describes in detail both the stochastic and deterministic aspects of the model.

2.3 The IP_3R Channel Model

Channel gating is the process by which channels change state or remain in the same state. The dynamics of this gating process are conventionally represented by a Markov chain model. [4] In the simplest possible scenario, a modeler might employ a two state model where one state represents the channel being open (1) and the other represents the channel being closed (2).

$$(1) \underset{k_{21}}{\overset{k_{12}}{\rightleftharpoons}} (2)$$

In this two-state model the a channel changes state according to forward and reverse rate constants (k_{12} and k_{21} respectively) that can be defined in terms of probability fluxes in an ensemble of identical and independent channels.

In the model of $[Ca^{2+}]_{cyt}$ oscillations presented here, we have chosen to employ a four-state IP_3R channel model that corresponds to a simplified version of the DeYoung-Keizer IP_3R model. This four-state model is minimal in two distinct ways. First, it represents the IP_3R as a collective entitty, as opposed to the DeYoung-Keizer model that explicitly modeled multiple IP_3R subunits. Secondly, the four-state model used here assumes IP_3 is at high concentration and thus IP_3 binding to the channel does not have to be explicitly modeled. [3]

In spite of these simplifications, the four-state model is similar to the DeYoung-Keizer model in that it accounts for the fast calcium activation and fast calcium inactivation of IP_3R. The transition-state diagram for this four-state model is

$$
\begin{array}{ccccc}
 & & k_{23}^{+}\mathrm{Ca}^{\eta} & & \\
\text{(open)} \quad 2 & & \rightleftharpoons & & 3 \quad \text{(inactivated)} \\
 & & k_{32}^{-} & & \\
k_{12}^{+}\mathrm{Ca}^{\eta} \quad \uparrow\downarrow \quad k_{21}^{-} & & & & k_{34}^{-} \quad \downarrow\uparrow \quad k_{43}^{+}\mathrm{Ca}^{\eta} \\
 & & k_{41}^{-} & & \\
\text{(closed)} \quad 1 & & \leftrightharpoons & & 4 \quad \text{(inactivated)} \\
 & & k_{14}^{+}\mathrm{Ca}^{\eta} & &
\end{array}
$$

When the channel is closed or inactive, Ca^{2+} ions cannot flow between the bulk ER and the bulk cytosol through the channel. The difference between "closed" and "inactivated" is that "inactivated" implies a longer mean dwell time. That is, the channel is likely to remain closed for a long time, but "closed" states can be very short-lived.

The four-state IP_3R model has both unimolecular (k_{21}, k_{32}, k_{34}, and k_{41}) rate constants and bimolecular (k_{12}, k_{23}, k_{42}, k_{14}) rate constants with units of s^{-1} and $\mu M^{-1}s^{-1}$ respectively. The unimolecular rate constants are appropriate when transitions between two states are calcium-indepenent. The bimolecular rate constants are used when the transitions between those states are calcium-dependent (that is, they involve the association of Ca^{2+} with the IP_3R). In cases of calcium-dependence, the Ca^{2+} concentration used is the value of the values of $[Ca^{2+}]_{cyt}^{d}$, the cytosolic domain concentration associated with that channel. The calcium-dependent rate constant between states 1 and 2 corresponds to "Ca^{2+} activation" and opening of the IP_3R channel. Conversely, the Ca^{2+}-dependent rate constant between

states 2 and 3 corresponds to Ca^{2+} inactivation of the IP_3R. Both calcium-activation and calcium-inactivation are experimentally observed phenomenon responsible for the well known bell-shaped curve. [2]

The process of calcium-activation and inactivation lead to oscillations in $[Ca^{2+}]_{cyt}$ in the models. Assuming the channels along the ER membrane start in the closed state, an increase in $[Ca^{2+}]_{cyt}$ causes transition into state 2, which in turn increases in $[Ca^{2+}]_{cyt}$. But this trend cannot last because the channel is also calcium-inactivated on a slower time scale. Therefore, when $[Ca^{2+}]_{cyt}$ gets large enough, the channels inactivate and remain closed for a long time. This allows the $[Ca^{2+}]_{cyt}$ to return to low values, the depleted $[Ca^{2+}]_{ER}$ to replenish, and the IP_3R channels return to state 1. The process can then repeat giving rise to oscillations in $[Ca^{2+}]_{cyt}$.

It is important to note that in this IP_3R model seven of the rate constants parameters are "free" (constrained only by experiment), while the eighth parameter is restricted by the thermodynamic constraint that detailed balance be satisfied when all the Ca^{2+} binding sites of the IP_3R experience the same Ca^{2+} concentration. That is,

$$k_{41} = \frac{k_{21}k_{32}k_{43}k_{14}}{k_{12}k_{23}k_{34}} \tag{1}$$

Also note that in the four-state model, calcium-dependent transitions occur at a rate proportional to $[Ca^{2+}]^{\eta}_{cyt}$. The exponent η corresponds to the cooperativity of Ca^{2+} binding to the IP_3R. For systems of $[Ca^{2+}]$ oscillations we assume that the cooperativity of Ca^{2+} binding is $\eta = 2$for both the Ca^{2+} activation and inactivation processes.

2.4 Monte Carlo Simulations

We employ the conventional Monte Carlo method to simulate the channel gating. The method determines the state of a given channel after a discrete time step (Δt) given that the original state of the channel is known. This method requires both the discretization of time into units of Δt and knowledge of the state of each channel at time $t = 0$. To determine if the channel changes state or not, a random number between 0 and 1 is compared to the product of Δt and the appropriate rate constant and, if required, a factor corresponding to the calcium dependence. If the random number is less than this product, the channel changes into the state indicated by the rate constant. Otherwise, if the random number is greater than that product, the channel remains in the same state. For example, in determining whether or not a channel in state 2 remains in state 2 or changes state into state 1 or into state 3, the method is as follows.

- Pick a pseudo-random number (x) uniformly distributed between 0 and 1.
- If $x < k_{21}\Delta t$, then change to state 1.
- else if $x < k_{21}\Delta t + k_{23}Ca^{\eta}\Delta t$, then change into state 3.
- else, the channel remains in state 2.

Note that the product of unimolecular rate constants with Δt ($s^{-1} \times s$) is a dimensionless number between 0 and 1, as is the product of the bimolecular rate constants with $[Ca^{2+}]^{\eta}_{cyt}$ and Δt ($\mu M^{-1}s^{-1} \times \mu Ms$).

This Monte Carlo method is known to be first-order accurate and is applied to every channel along the length of the membrane at each time step Δt throughout the entire sim-

ulation. When Δt is very small (on the order of 1×10^{-5} seconds, as it must be for reasons discussed later), the number of calculations to run a simulation gets to be extremely large resulting in longer run times for the simulations.

2.5 The Mass Balance Equations

The deterministic component of the model of intracellular Ca^{2+} handling the differential "mass balance equations" that determine the rate of change of $[Ca^{2+}]$ in each of the four compartments as a function of time. These equations include both diffusion terms and reaction terms. The diffusion terms describe the diffusion of $[Ca^{2+}]$ in each compartment along the length of the ER membrane. The reaction terms correspond to the stochastic gating of the channel states. Because $[Ca^{2+}]$ is changing with respect to time in four compartments, there are four mass balance equations that take the form

$$\frac{\partial [Ca^{2+}]_{cyt}}{\partial t} = D\frac{\partial^2 [Ca^{2+}]_{cyt}}{\partial x^2} + J_{cyt} + J_{leak} - J_{pump} \tag{2}$$

$$\frac{\partial [Ca^{2+}]_{ER}}{\partial t} = D_{ER}\frac{\partial^2 [Ca^{2+}]_{ER}}{\partial x^2} + \frac{1}{\lambda}(J_{pump} - J_{leak} - J_{ER}) \tag{3}$$

$$\frac{\partial [Ca^{2+}]^d_{cyt}}{\partial t} = \frac{1}{\lambda_1}(J_{rel} - J_{cyt}) \tag{4}$$

$$\frac{\partial [Ca^{2+}]^d_{ER}}{\partial t} = \frac{1}{\lambda_2}(J_{ER} - J_{rel}) \tag{5}$$

Note that the Equation 2 and 3 contain a diffusion term while Equations 4 and 5 do not. This implies that diffusion between the domain compartments along the length of the membrane must occur between the bulk.

The λ factors appearing in Equations 3, 4 and 5 are volumetric scaling constants given by the ratio of cytosolic volume to the volume of each compartment. These scaling terms are needed because the volumes occupied by the compartments are different and it is the total number of Ca^{2+} ions (not their concentration) that is conserved in the "closed cell" model with no plasma membrane fluxes.

The flux equations that appear in Equations 2 - 5 are given by

$$J_{leak} = v_{leak}([Ca^{2+}]_{ER} - [Ca^{2+}]_{cyt}) \tag{6}$$

$$J_{pump} = \frac{v_{pump}([Ca^{2+}]_{cyt})^2}{k_p^2 + ([Ca^{2+}]_{cyt})^2} \tag{7}$$

$$J_{rel} = p_o v_{rel}([Ca^{2+}]^d_{ER} - [Ca^{2+}]^d_{cyt}) \tag{8}$$

$$J_{cyt} = v_{cyt}([Ca^{2+}]^d_{cyt} - [Ca^{2+}]_{cyt}) \tag{9}$$

$$J_{er} = v_{er}([Ca^{2+}]_{ER} - [Ca^{2+}]^d_{ER}) \tag{10}$$

In equation 8, the *po* term represents whether or not the channel is open at that time. If open, $p_o = 1$ then Ca^{2+} ions flow between the domain compartments, otherwise $p_o = 0$, the channel is closed, and Ca^{2+} ions cannot flow between these compartments. Equations 9 and 10 do not depend on whether or not the channels are open, but they do depend on the concentration gradient between their respective bulk and domain concentrations, which will only be different during (or immediately following) channel opening. Most of these fluxes depend on a concentration gradient. The exception is equation 7, which represents the SERCA Ca^{2+}-ATPase (i.e pumps) flux that works against the concentration gradient between the bulk ER and the cytosolic Ca^{2+} concentration. The flux, J_{pump} replenishes $[Ca^{2+}]_{ER}$ and is a sigmoidal function of $[Ca^{2+}]_{cyt}$.

The parameters in these equations for the fluxes ($v_{leak}, v_{pump}, k_p, v_{rel}, v_{cyt}$ and v_{ER}) depend on the particular cell type one is modeling. Some have been estimated experimentally while others are essentially determined by known quantities such as the resting Ca^{2+} concentrations in the bulk compartments and are presented in Table 1.

2.6 The Mesh

A mesh is an important aspect of modeling a spatially dependent system. In this case, the mesh points are the specific locations along the length of the membrane where the Ca^{2+} concentrations will be approximated by our numerical scheme. The length of the membrane (L) is divided into N equal regions of length $l = \frac{L}{N}$. To incorporate the location of the channels in the mesh, we introduce the idea of channel clusters. Channel clusters are areas along the membrane consisting of large numbers of release cites clustered together. These regions of length l each contain x (where $x = y + z$) mesh points, the first y of which correspond to release sites, while the remaining z mesh points correspond to the gaps between the channel clusters where intracellular channels are absent. That is, each group of y mesh points represents a channel cluster along the ER membrane. The result is a distribution of regularly spaced channel clusters along the length of the cell. Increasing N results in a larger number of release sites, while maintaining the faction of the membrane occupied by a release site constant ($\frac{y}{y+z}$).

There are a total of $J = Nx$ mesh points, each of which can be indexed with a subscript j. At each mesh point we solve for the four Ca^{2+} concentrations. As time evolves, the structure of the mesh is maintained but the four concentrations at each spatial location are updated

Figure 2

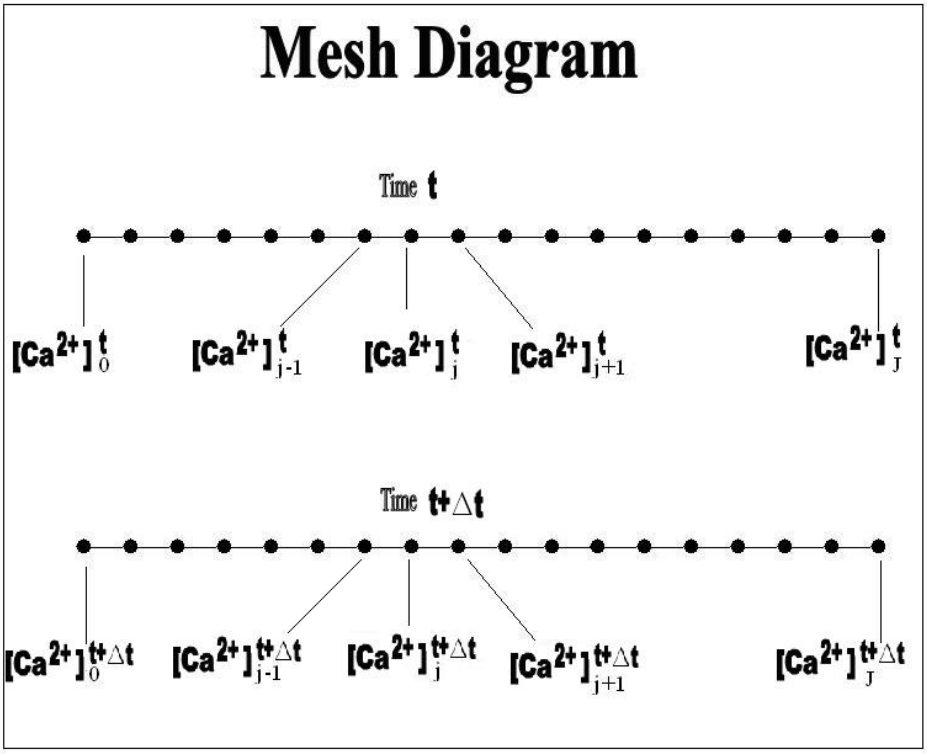

via the diffusion and reaction terms of the mass balance equations. The mesh diagram has periodic boundary conditions (meaning that the mesh point after the Jth point is identified with the first mesh point), a choice that minimizes "edge effect" in the model that are not of interest.

2.7 Modeling Ca^{2+} Diffusion

For simplicity we implemented an explicit numerical scheme to solve Equations 2- 5. Taking the dependent variable $[Ca^{2+}](x,t)$, as an example, the scheme uses the values of $[Ca^{2+}]_{cyt}(x,t)$ to predict the unknown values $[Ca^{2+}]_{cyt}(x,t+\Delta t)$. This method requires the discretization of both time and space, the later being provided by the mesh diagramed in

Figure 2. For simplicity, the time-step is chosen to be a fixed value Δt, rather than adaptive.

To solve for the diffusion terms in the mass balance equations, we use a forward first difference in time (first order accurate) and a centered second difference in space (second oder accurate) approximation given by

$$\left.\frac{\partial[Ca^{2+}]}{\partial t}\right|_{j,t} \approx \left.\frac{\partial^2[Ca^2]}{\partial x^2}\right|_{j,t} \frac{[Ca^{2+}]^t_{j-1} - 2[Ca^{2+}]^t_j + [Ca^{2+}]^t_{j+1}}{\Delta x^2} \tag{11}$$

Substituting and rearranging Equation 11 to solve for the unknown mesh point $[Ca^{2+}]^{n+1}_j$, find

$$[Ca^{2+}]^{t+\Delta t}_j = [Ca^{2+}]^t_j + \frac{D\Delta t}{\Delta x^2}([Ca^{2+}]^t_{j-1} - 2[Ca^{2+}]^t_j + [Ca^{2+}]^t_{j+1}) \tag{12}$$

This method is applied at each mesh point and for each of the four compartments of the model. There is a condition of crucial importance on the numerical stability of this explicit numerical scheme: the time step must be small enough to satisfy the following inequality

$$\frac{D\Delta t}{\Delta x^2} < \frac{1}{2}. \tag{13}$$

Thus, when modeling the mass balance equations it is imperative to choose the relative size of D,Δx and Δt appropriately.

3 The Spatio-Temporal Model

The spatio-temporal model is a complete model in the sense that it explicitly accounts for both space (along the length of the ER membrane) and time. The PDA model is a

simple model in that it ignores the spatial dependence. One goal was to compare a Monte Carlo version of the PDA model to the corresponding one-dimensional spatial model in order to clarify the effect of ignoring space on the accuracy of the probability density approach. Therefore, all the parameters in both models will be the same and the only difference will be the inclusion of the spatial dependence in the complete spatio-temporal model (hereafter referred to as the 1D model). The parameters common to both models are given in Table 1.

The 1D model is built with the intention of limiting the dependence of $[Ca^{2+}]$ on the location along the membrane. The less dependent on location, the more likely the two models are to agree. In this 1D model, there will be $N = 1000$ channel clusters. In addition, there will be no space between these channel clusters, therefore every mesh point corresponds to a release site. This is equivalent to setting $z = 0$ in the formulation of the mesh diagram. This results in an ER membrane that is entirely covered with channel clusters. The serves to reduce the dependence of $[Ca^{2+}]$ on the location along the membrane since every mesh point is identical. The two channel-independent fluxes J_{pump} and J_{leak} are also present at all locations along the membrane. Concentrations in neighboring domains do not directly interact with each other via diffusion, but may influence on another via the bulk cytosolic and ER Ca^{2+} concentrations. Figure 3 is a visual schematic of the final 1D model with a resistor symbol indicating model fluxes.

Initially we force 10% of the channel clusters to be in state 1, while the remaining 90% of the channels are in state 4. The 10% of channel clusters in state 1 are randomly distributed along the length of the membrane. The initial $[Ca^{2+}]$ values are homogeneous along the length of the membrane with $[Ca^{2+}]_{cyt} = [Ca^{2+}]^d_{cyt} = 0.1$ μM and $[Ca^{2+}]_{ER} = [Ca^{2+}]^d_{ER} = 9$

Table 1

Parameter	Value	Units
N	1000	
k_{12}	500	$\mu M^{-1}s^{-1}$
k_{23}	4	$\mu M^{-1}s^{-1}$
k_{34}	1000	s^{-1}
k_{14}	4	$\mu M^{-1}s^{-1}$
k_{43}	500	$\mu M^{-1}s^{-1}$
k_{32}	0.1	s^{-1}
k_{21}	1000	s^{-1}
k_{41}	$\frac{k_{21}k_{14}k_{43}k_{32}}{k_{12}k_{23}k_{34}}$	s^{-1}
η	2	——

μM.

To further reduce the spatial-dependence of $[Ca^{2+}]$ we incorporate parameters to make the spatial-profile of $[Ca^{2+}]$ at any given time to be as flat as possible. A flat spatial profile would indicate that regardless of location along the membrane, the $[Ca^{2+}]$ value is more or less the same. To promote this spatial homogeneity, we make the diffusion between the bulk mesh points very fast along the length of the membrane (D and D_{ER}). Figure 4 shows the effect of the diffusion coefficients on the spatial profiles two seconds into the simulation.

We have found it informative to report the data from the 1D simulations using three different types of graphs: $[Ca^{2+}]_{cyt}$ vs. time, spatial profiles and histograms.

3.1 $[Ca^{2+}]$ as a function of time

By explicitly keeping track of the various concentrations at each time, we can plot the time evolution of the average values of $[Ca^{2+}]_{cyt}$ as in Figure 5.

Figure 3: Schematic of the 1D model

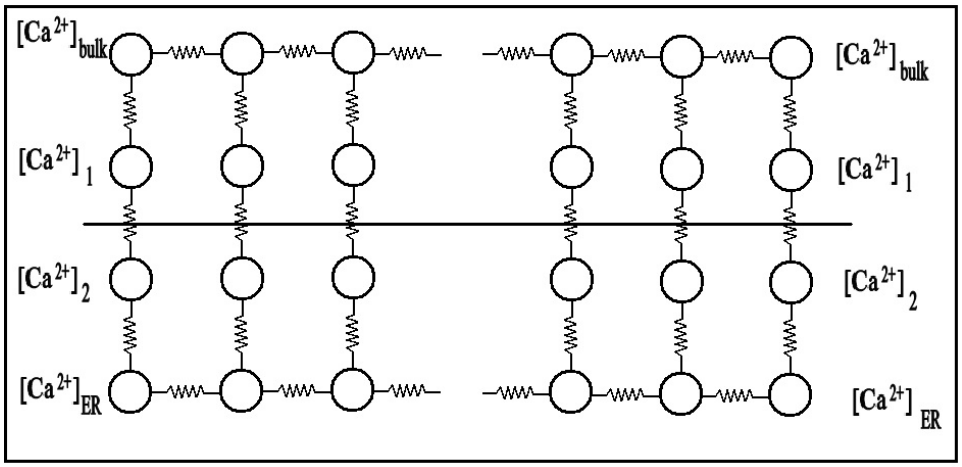

Figure 4: The figure on the left shows the spatial profile of the model at a time $t = 2$s with diffusion coefficients $D = D_{ER} = 50\mu\text{m}^2 s^{-1}$. The figure on the right shows the spatial profile of the same model except with diffusion coefficients $D = D_{ER} = 500\mu m^2 s^{-1}$. Notice that the figure on the right is much flatter than the figure on the left. The solid line in these figures is the $[Ca^{2+}]_{cyt}$ while the x's are values of $[Ca^{2+}]^d_{cyt}$ at those locations.

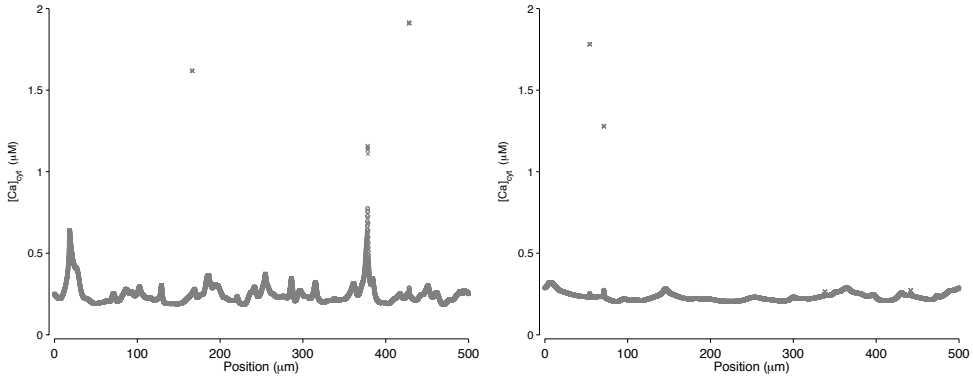

Figure 5: Plots of $[Ca^{2+}]_{cyt}$ as a function of time in the four-compartment 1D spatial model. This plot shows stochastic oscillations mediated by fast Ca^{2+} activation and slower Ca^{2+} inactivation of IP_3Rs

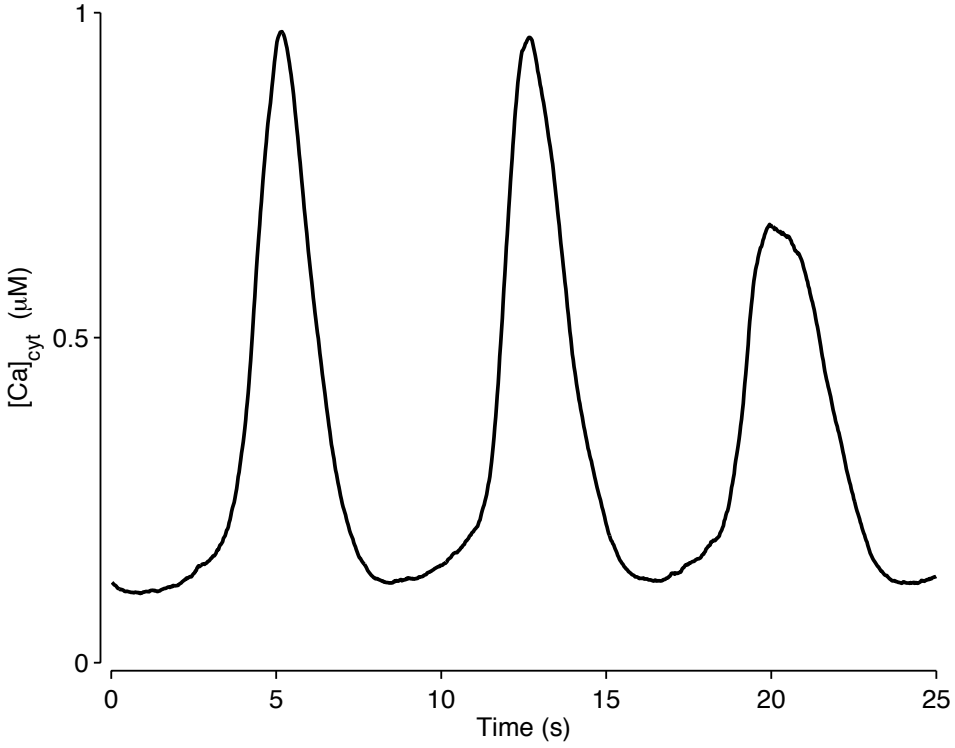

To make these figures, we have to take the average $[Ca^{2+}]_{cyt}$ value along the length of the membrane at each time. For simulations where the $[Ca^{2+}]$ along the length of the membrane is fairly homogeneous, as is the case for extremely fast diffusion, the averaging does not introduce very much error. The more non-homogeneous the spatial profiles, the more error is introduced by the averaging. Therefore, the averaging will constitute one source of discrepancy between the 1D model and the PDA model.

Figure 5 shows the calcium oscillations that we have been trying to model. The fairly regular frequency indicate that the model is working properly. That is, all the channel clusters are gating appropriately and all the concentrations are changing as we would expect.

These figures will serve as one way of comparing the results from the PDA and 1D modeling approach

3.2 Spatial Profiles

Spatial profiles are a good way of seeing how $[Ca^{2+}]$ is dependent on the location along the membrane as well as the state of the corresponding release site. Figure 6 gives an example of how we plot the spatial profile of a simulation at a particular time. Figure 6 contains three subplots. The top subplot shows both $[Ca^{2+}]_{cyt}$ (o's) and $[Ca^{2+}]^d_{cyt}$ (x's) at each mesh point along the length of the membrane (in this case 500 μm). For most of the mesh points, the bulk and domain cytosolic concentrations agree, which is why see one line and a few points outside that line. The x's above the dominant line show that $[Ca^{2+}]^d_{cyt} > [Ca^{2+}]_{cyt}$ at those mesh points. In addition, the x's indicate that the channel cluster is in the open state.

The second subplot plots the state of each channel cluster along the length of the membrane. In this model of 1000 channel clusters, there are a thousand channel clusters, each of which independently transition between the four states. In Figure 6 most of the channel clusters are inactivated, while a small percentage remain open.

The bottom subplot shows $[Ca^{2+}]_{er}$ (o's) and $[Ca^{2+}]^d_{ER}$ (x's) at each point along the length of the ER membrane.

3.3 Histograms

At any given time, there are 1000 channel clusters each of which can be in any of the four channel states. The histograms require segregating the channel clusters according to

Figure 6: Spatial Profile of a 1000 channel cluster model at time $t = 5s$. Note that channel clusters in state 2 correspond to elevated $[Ca^{2+}]^d_{cyt}$ values in the top graph, which serve to increase $[Ca^{2+}]_{cyt}$ at those locations. Also notice the inverted symmetry between the top and bottom plots.

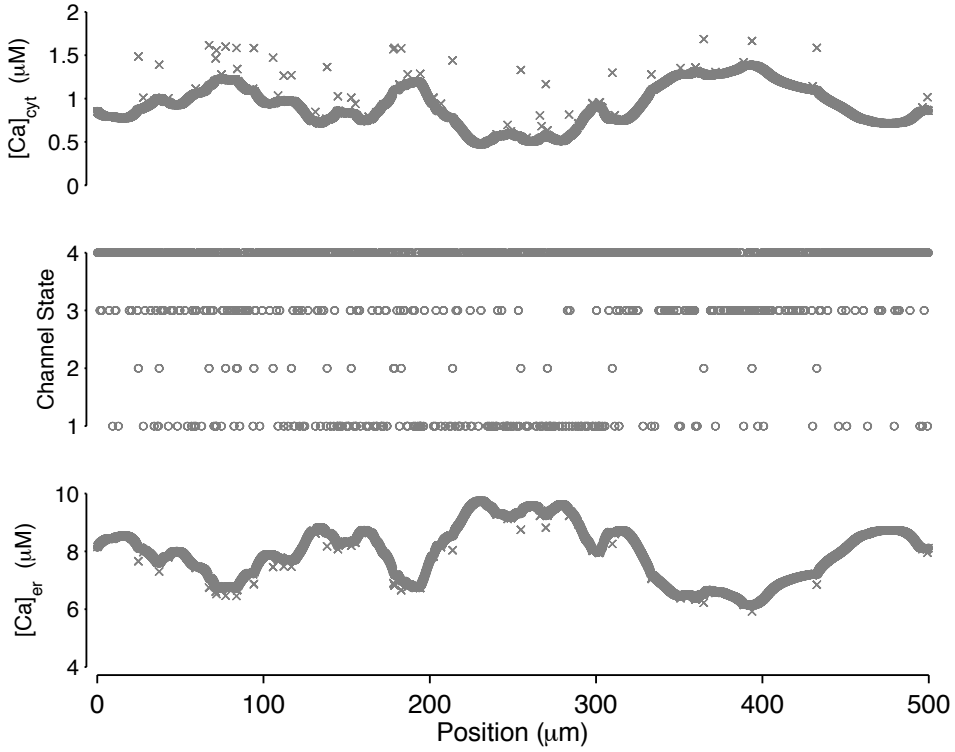

channel state and then plotting the distribution of the domain values in each of those states. Projecting the distribution of the $[Ca^{2+}]^d_{cyt}$ values down onto a histogram that plots the number of channel clusters with $[Ca^{2+}]^d_{cyt}$ values within particular value ranges, gives us a probability of any channel cluster being in the state x with a certain $[Ca^{2+}]^d_{cyt}$. Similarly, projecting the distribution of the $[Ca^{2+}]^d_{cyt}$ values across onto a histogram that plots the number of channel clusters with $[Ca^{2+}]^d_{ER}$ values within particular value ranges, gives us a probability of any channel cluster being in the state x with a certain $[Ca^{2+}]^d_{ER}$.

Figures 7 and 8, show the histograms for the crest and trough of the first oscillation in Figure 5. Figure 7 corresponds to $t = 5$ s and Figure 8 corresponds to $t = 7$ s. The resulting histograms are particularly informative. It can tell us the probability of any channel being open at these times, or the probability of any channel having a particular $[Ca^{2+}]^d_{cyt}$ or $[Ca^{2+}]^d_{ER}$ value. In these figures, n gives the number of channels (out of 1000) in each state.

In Figure 7, nearly all of the channel clusters have inactivated. At this time, the $[Ca^{2+}]$ has nearly reached its maximum, therefore most $[Ca^{2+}]^d_{cyt}$ values are larger at this time than when $[Ca^{2+}]_{cyt}$ is low. This is verified in comparing Figures 7 and 8, where nearly all of the $[Ca^{2+}]^d_{cyt}$ values in Figure 7 are larger than the $[Ca^{2+}]^d_{cyt}$ values in Figure 8.

In Figure 8, virtually all of the channel clusters are still in the inactive state and the domain concentrations have returned to their original values as specified by the initial conditions. At this time, the system is ready to begin another oscillation.

Figure 7

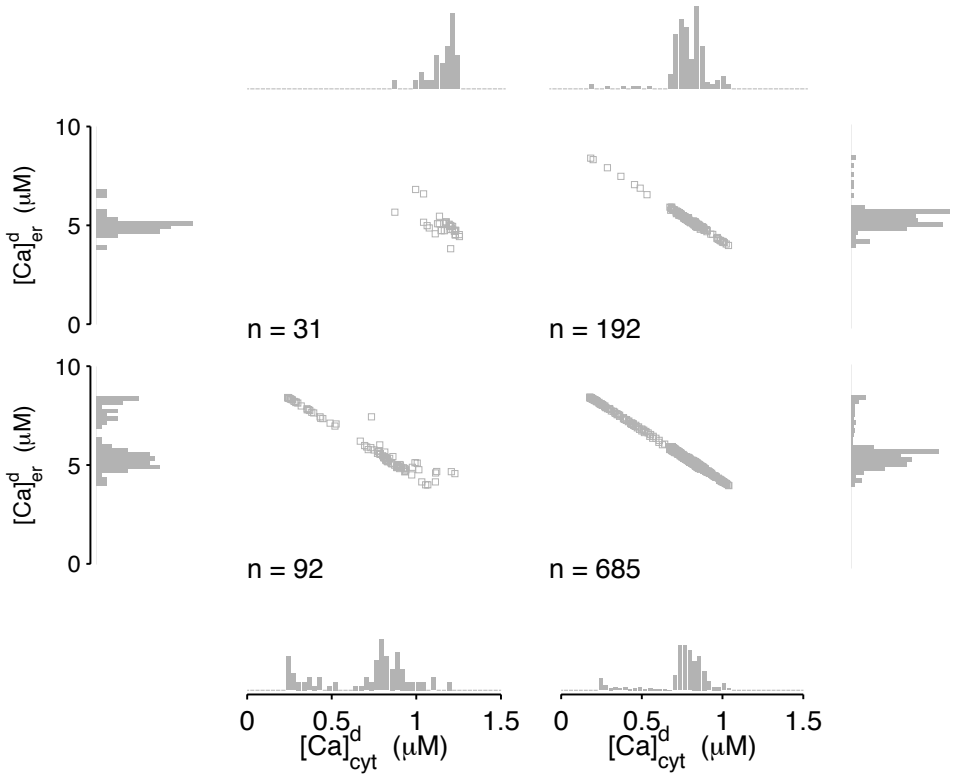

Figure 8

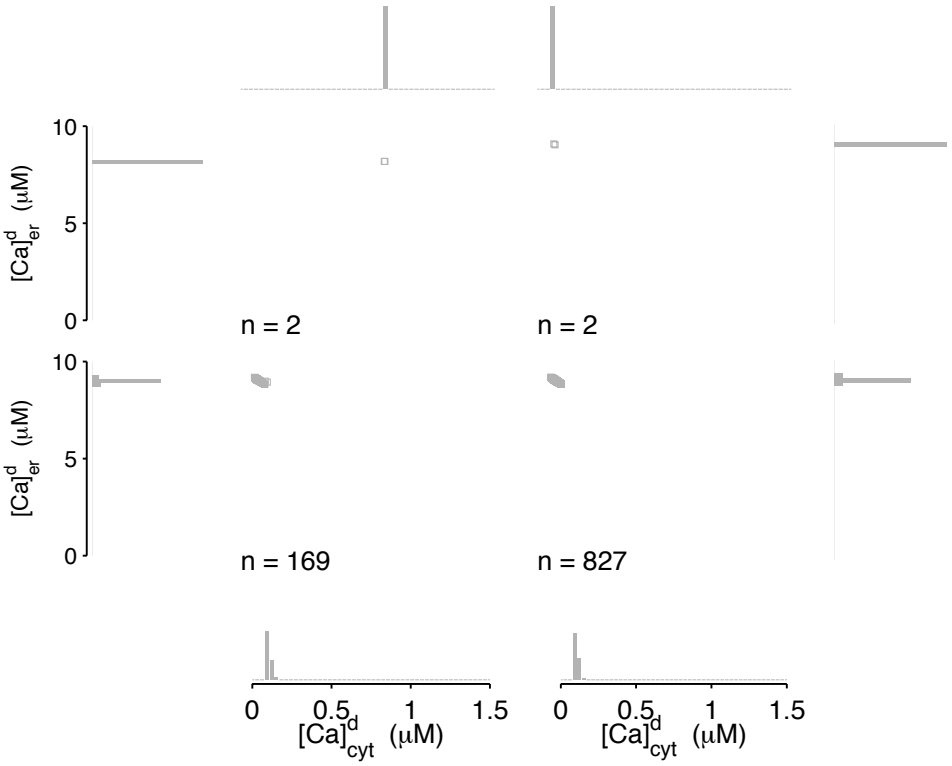
10
5
0
[Ca]$^{d}_{er}$ (μM)
n = 2
n = 2
10
5
0
[Ca]$^{d}_{er}$ (μM)
n = 169
n = 827
0
0.5
1
1.5
[Ca]$^{d}_{cyt}$ (μM)
0
0.5
1
1.5
[Ca]$^{d}_{cyt}$ (μM)

Figure 9: Results from the PDA model (solid line) and the 0D Monte Carlo model (gray boxes) with identical parameters. Graph provided by Blair Williams

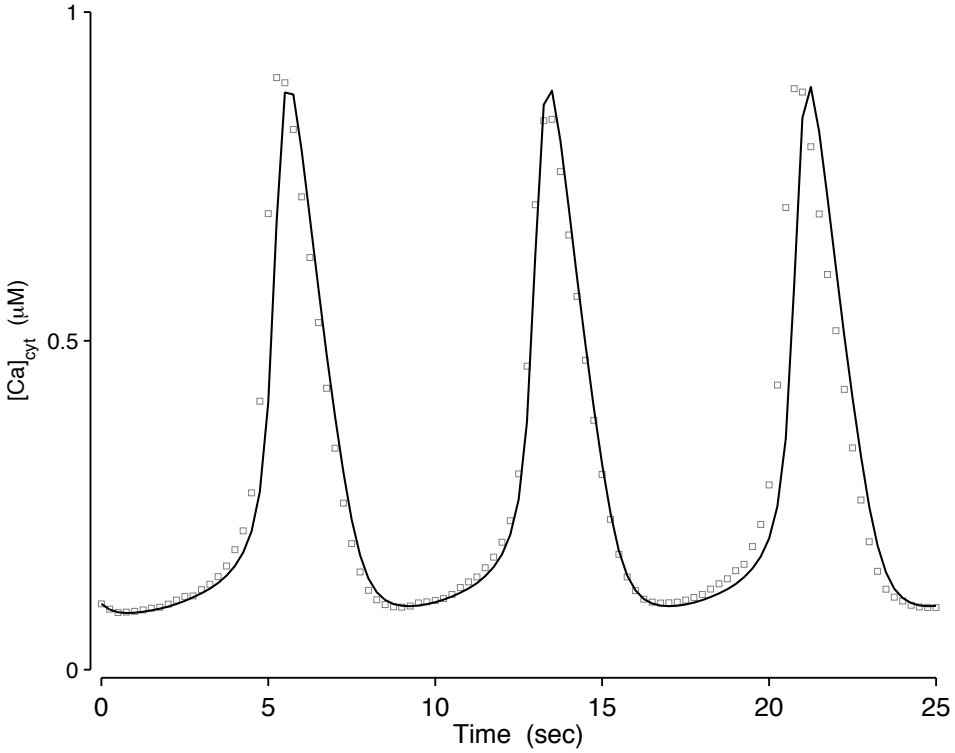

4 The Comparison and Results

4.1 PDA and Zero-Dimensional Monte-Carlo Model Equivalence

The PDA model outputs data that is fairly difficult to compare to the 1D Monte-Carlo model. Therefore, we will compare the 1D model to a Zero dimensional monte-carlo model (0D model) that is equivalent to the PDA results. To show this equivalence see Figure 9. The black solid line corresponds to the results from the PDA model. The gray boxes correspond to results from the 0D Monte Carlo model. There is significant agreement so we can accurately compare the 1D model to the PDA model indirectly through a comparison between the 1D model and the 0D model

4.2 Comparison Techniques

To get a sense of how the 0D model's exclusion of the spatial dimension along the length of the membrane affects its accuracy, we will simulate the 1D model with two distinct parameter sets. The first set will be for fast diffusion between bulk concentrations along the length of the membrane. As discussed earlier, we expect fast diffusion to reduce the dependence of $[Ca^{2+}]$ on the location along the length of the membrane. The second parameter set will be for slow diffusion between bulk concentrations along the length of the membrane. By slowing down this diffusion, we expect the concentrations to be more dependent on location along the membrane. That is, we expect more variance between concentrations at different locations along the membrane. By performing the simulations in these two parameter sets, we can at least get a sense of how the agreement between the two models depends on the spatial dependence of the 1D model.

4.3 Fast Diffusion

To simulate fast diffusion along the length of the membrane, we set $D = D_{ER} = 500$. For Diffusion coefficients this large, we had to restrict our time step Δt to be very small as required by Equation 13. In our model, $\Delta x = 0.1\mu$m. Therefore, Equation 13 requires $\Delta t = 10^{-5}s$. These simulations took about 14 hours per run on an Apple X-serve G5 with dual 2.3 GHz processors with G5 PowerPC chips and 2GB of RAM.

Figure 10 puts the plots of $[Ca^{2+}]_{cyt}$ vs. time for both models together on the same scale. A visual comparison of these two plots show a few key and obvious similarities. First, both graphs have three oscillations and occur at roughly the same frequency. Neither graph

Figure 10: $[Ca^{2+}]_{cyt}$ for both the 1D (solid) and the 0D (dotted) models.

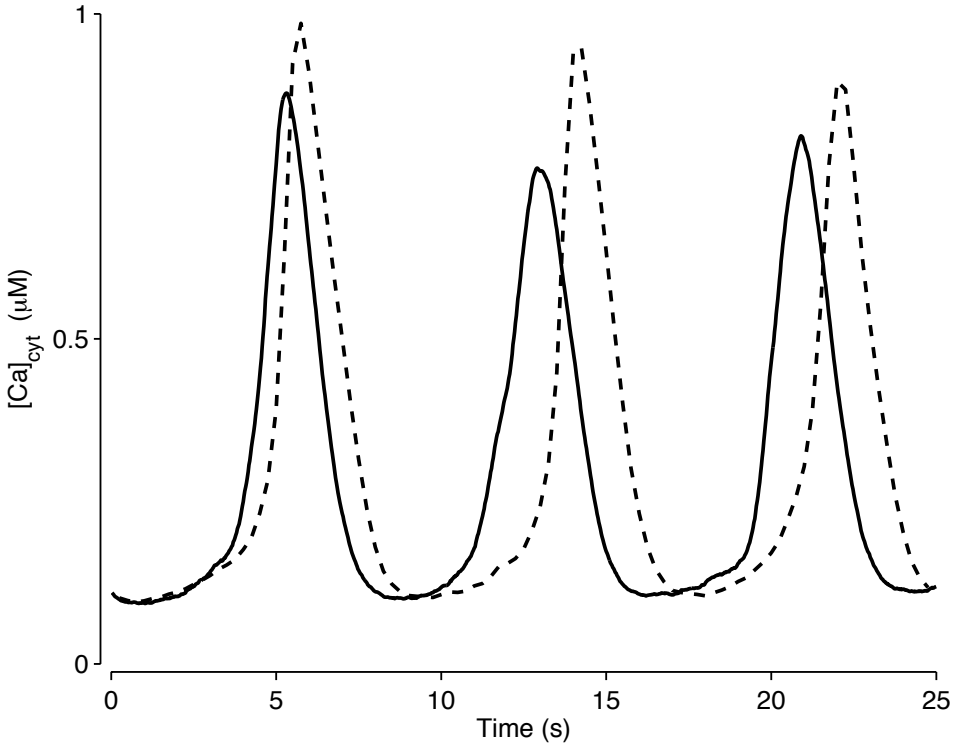

has all of its peaks reach the same amplitude. In the 0D simulation, the first two peaks reach about 0.9 μM while the last peak only goes up to about 0.8 μM. In the 1D simulation, the first peak reaches about 0.8 μM while the other two peaks only reach 0.7 μM. These similarities indicate that the two models are showing equivalent dynamics (the oscillations) with nearly the same properties (amplitude and frequency). Despite this level of agreement, there are also some obvious dissimilarities between the two. The amplitudes in each simulation disagree. The amplitudes in the 0D model are higher than the amplitudes in the 1D model. Finally, though the oscillations have nearly identical frequencies, they oscillations are out of sync. In the 0D model, the amplitude of the first oscillation peaks at about 6 s. The amplitude of the first oscillation in the 1D model peaks a little earlier at about 5 s. There is every reason to believe that if the diffusion coefficients were made larger, the spatial profiles of the bulk cytosolic and ER Ca^{2+} concentrations would become more uniform, and the 1D model would exhibit responses even more similar to the 0D model.

4.4 Slow Diffusion

To simulate slow diffusion along the length of the membrane, we set $D = D_{ER} = 50$ $\mu\text{m}^2 s^{-1}$, ten times slower than in the previous example. Using diffusion coefficients that are ten times smaller allows for time steps that are ten times larger, according to Equation 13. Consequently these simulations ran ten times faster than did the simulations with faster diffusion.

Looking at Figure 11 it is clear that there is considerably less agreement between the 0D model and slow diffusion 1D model than there is between the 0D model and the fast diffusion

Figure 11: $[Ca^{2+}]_{cyt}$ for both the slow 1D (solid) and the 0D (dotted) models.

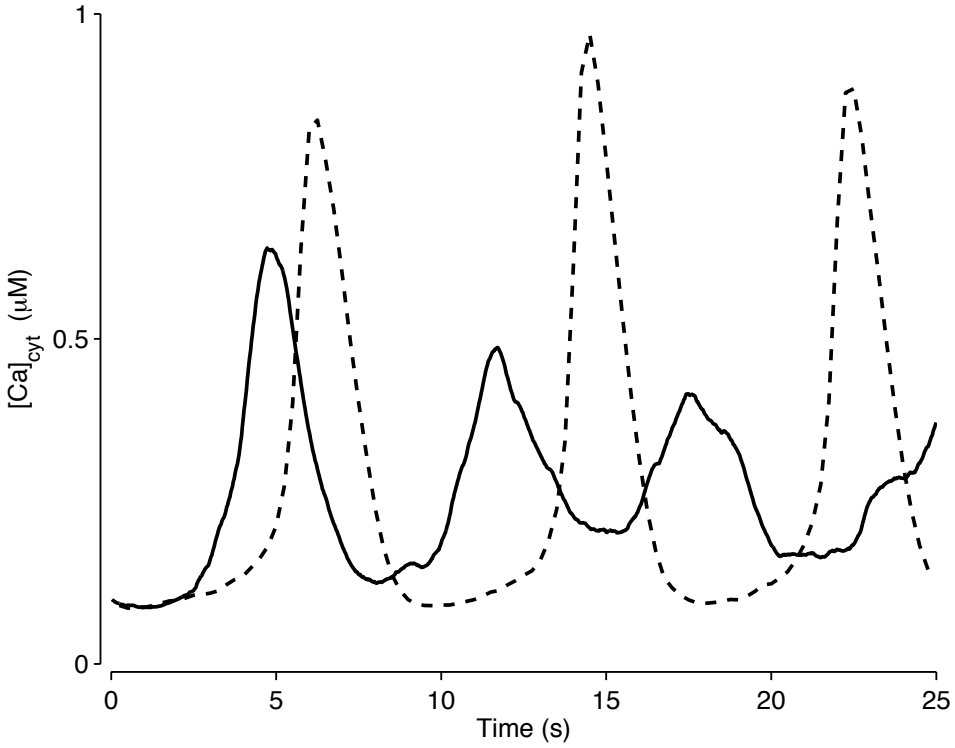

1D model. In this case, the similarities seen before are not seen here. The two graphs in Figure 11 do not have even comparable amplitudes. The peaks in the 0D simulation have amplitudes near 1 μM, while the tallest peak in the 1D model has an amplitude of about 0.7 μM with all the later peaks at even lower amplitudes. Furthermore, not even the number of oscillations between these two models is consistent. As before, there are only three oscillations in the 0D simulation. This 1D model, however, shows almost four oscillations. Finally, one does not even see the even spacing between the oscillations in this 1D simulation, where as the fast diffusion 1D model had much more evenly spaced oscillations.

5 Discussion

We have shown reasonable levels of agreement between the 0D and 1D models in the fast diffusion case, and further shown that the value of the diffusion constant in the 1D model plays a significant role in this agreement. The faster the diffusion in the 1D model, the less $[Ca^{2+}]$ depends on the location along the membrane. This is because the fast diffusion serves to homogenize the spatial profile. In the case of the slower diffusion in the 1D model, the $[Ca^{2+}]$ varied more significantly along the length of the membrane. Figure 4 shows the differences in the spatial profiles between the two 1D simulations. These spatial profiles are taken at times where there is a large amount of channel activity to show maximum variance in each case. Notice that the model with the faster diffusion is more spatially homogeneous than is the model with the slower diffusion.

In this study, even the fast 1D model with $D = D_{ER} = 500\mu m^2 s^{-1}$, while more homogeneous than the slower diffusion 1D model, is still not completely homogeneous. Figure 12

Figure 12: Spatial profile of the 1D model with $D = D_{ER} = 500\mu m^2 s^{-1}$. This profile shows that even with the faster diffusion, there is still substantial variance.

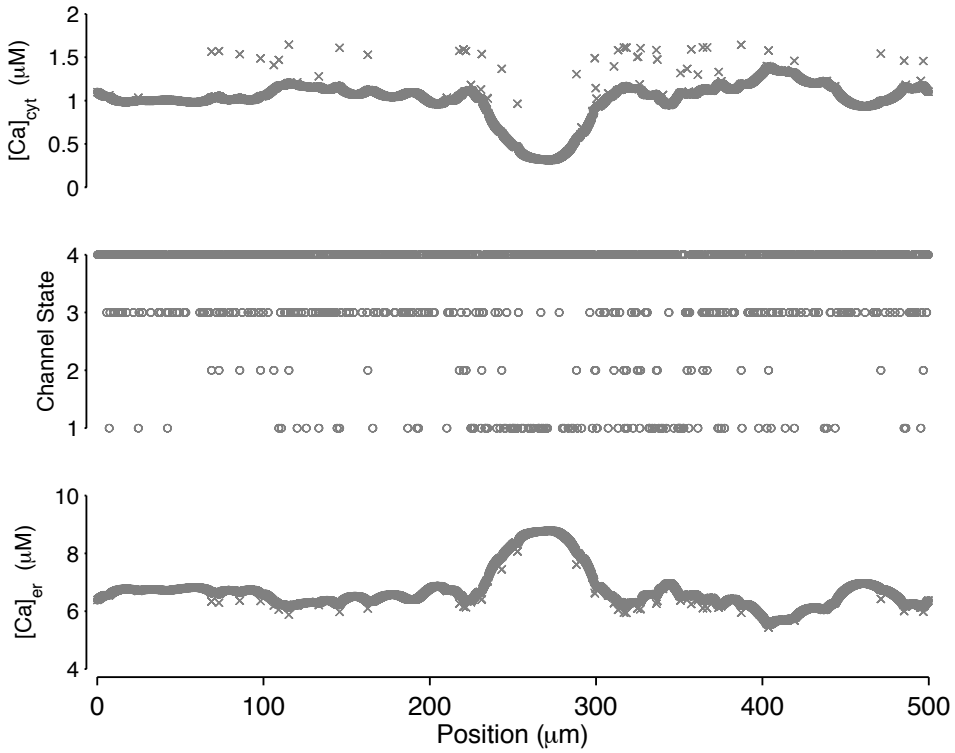

shows that the variance in $[Ca^{2+}]$ along the membrane ranges from values as low as 0.4 μM to values as high as 1.1 μM. The disagreement shown in Figure 10 is probably due to the lack of complete homogeneity in the 1D model. We suspect, that if the diffusion coefficients were increased still further the homogeneity would increase and there would be more agreement between the 1D and 0D case. These results to support the claim that the two models would agree in the case of near total homogeneity. For the first two seconds in the fast diffusion 1D model, the spatial profile nearly totally homogeneous (Figure 13). Figure 10 shows that at time $t = 2s$ the concentrations are nearly identical.

However, the restriction given by Equation 13 makes this a very computationally intensive simulation. Increasing the diffusion coefficients by a factor of ten would proportionally

Figure 13: Spatial profile for the 1D model with fast diffusion at time $t = 2s$. The homogeneity seen in this figure suggests that the homogeneity of the model depends on the dominant state of the system. In this case, most of the channel clusters are inactive.

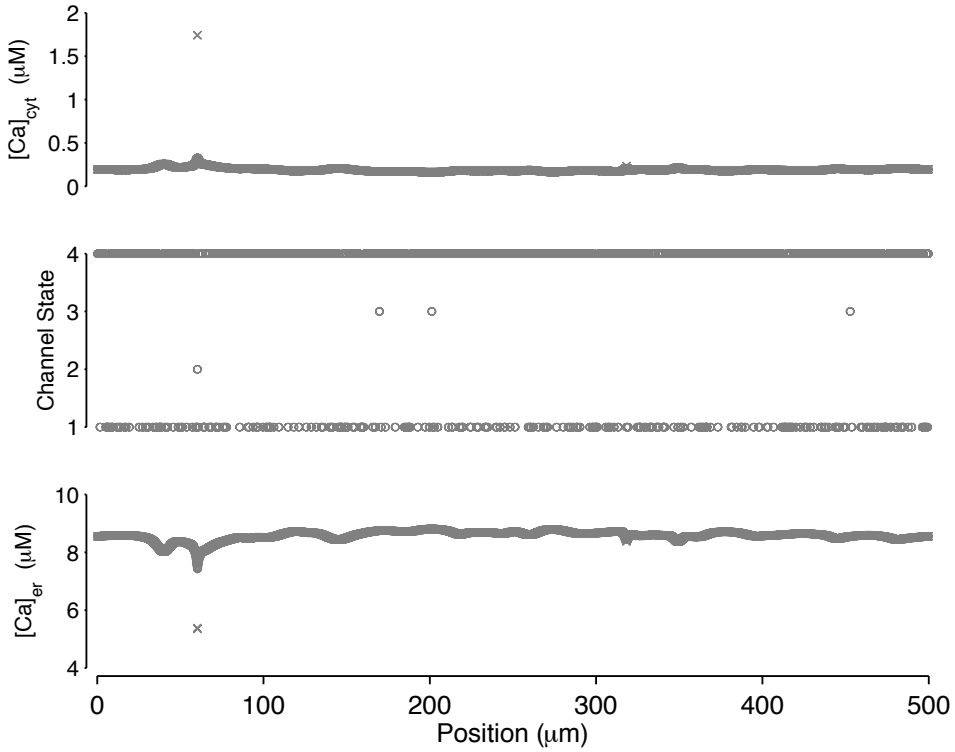

decrease the maximum time step by a factor of ten. The simulations with $D = D_{ER} = 500\mu m^2 s^{-1}$ already take about 14 hours, so faster diffusion will result in simulations that take several days. Even diffusion coefficients of $D = D_{ER} = 5,000\mu m^2 s^{-1}$ do not guarantee sufficient homogeneity. It is very possible that in order to see complete agreement we would have to run simulations that take about a week or so each.

There is a way to shorten the length of the simulations even with these extremely large diffusion coefficients. The restriction given by Equation 13 is a result of using an explicit method for calculating diffusion along the length of the membrane. By replacing this explicit method with an implicit Crank-Nicholson-like method, we would remove this restriction on Δt. Consequently we could take larger time steps allowing for faster simulations. Using this approach, the diffusion coefficients could be increased until they are large enough to produce nearly absolute homogeneity in the spatial profiles of the 1D model. This would be a natural extension of this project.

There is abundant experimental evidence that the free Ca^{2+} diffusion coefficients in living cells are in the rang 100-500$\mu m^2 s^{-1}$. Because the high end of this physiological range corresponds to the fast diffusion 1D calculations shown above (Figure 10), the limited convergence observed between the 1D and 0D models suggests that not explicitly accounting for spatial aspects of calcium signaling may be a significant limitation of the probability density approach applied to models of IP_3-dependent Ca^{2+} signaling.

Finally, it is interesting to note that a naive calculation of the diffusion rate that might

be considered fast in this problem would be given by

$$D > \frac{L^2}{T} \tag{14}$$

where L is a characteristic spatial scale (e.g., the length of the cell or the length of on release site) and T is a characteristic time scale (e.g., the period of an oscillation or one of the rate constants in the IP_3R model). Using the length of a small cell ($10\mu m$) and oscillation period of T = 10 s, this gives D>10 $\mu m^2 s^{-1}$. The simulations presented here are 500 μm in length, a value realistic for a very large cell such as the Xenopus laevis oocyte. It would be interesting to repeat these calculations on a shorter spatial domain to see if this minimizes the observed differences between the 1D spatial model and the 0D reduction.

6 Acknowledgments

I would first like to thank Dr. Gregory Smith for his agreement to allow me to work with his lab at Applied Science and for being my advisor. He allowed me to attend both of his graduate seminars on mathematic physiology through which I learned most of the information needed in this project. Dr. Smith also helped me with programming and coding in Matlab. I would also like to thank the graduate students in his lab for their help. Blair Williams helped me style me figures in a more presentable and informative format. He also provided the code for the 0D model. Jeff Groff provided me with the style sheet for this paper.

References:

[1] MJ Berridge. Elementary and global aspects of Ca^{2+} signalling. *J Physiol (London)*, 499(Pt 2):291–306, 1997.

[2] I Bezprozvanny, J Watras, and BE Ehrlich. Bell-shaped Ca^{2+}-response curves of Ins(1,4,5)P3- and Ca^{2+}-gated channels from endoplasmic reticulum of cerebellum. *Nature*, 351(6329):751–4, 1991.

[3] GW De Young and J Keizer. A single-pool inositol 1,4,5-trisphosphate-receptor-based model for agonist-stimulated oscillations in Ca^{2+} concentration. *Proc Natl Acad Sci USA*, 89(20):9895–9, 1992.

[4] GD Smith. Modeling the stochastic gating of ion channels. In CP Fall, ES Marland, JM Wagner, and JJ Tyson, editors, *Computational Cell Biology*, pages 291–325. Springer-

Verlag, 2002.

[5] C Tignanelli. *The effect of residual* Ca^{2+} *on the stochastic gating of* Ca^{2+}*-regulated* Ca^{2+} *channels*. The College of William and Mary, Williamsburg, VA, 2005.